Unsteady Two-Phase Flow Measurements in Surges and Dam Break Waves

Hubert Chanson[1]

1: Department of Civil Engineering, University of Queensland, Brisbane Qld 4072, Australia,
h.chanson@uq.edu.au

Abstract   Flood waves resulting from dam breaks and flash floods have been responsible for numerous losses. In the present study, sudden flood releases were investigated down a large stepped waterway initially dry. A new experimental technique was developed to obtain instantaneous void fractions, bubble count rates and velocities. Unsteady air-water flow properties were recorded with arrays of conductivity probes. The results showed a strong aeration of the surge leading edge. Instantaneous velocity measurements indicated an unsteady turbulent boundary layer region with a potential flow above. In the unsteady boundary layer, void fraction and velocity data suggested a ratio of bubble diffusivity to eddy viscosity of about unity. Practically, the study provides new information on free-surface aeration in surging waters in channels and on beach slopes.

1. Introduction

Flood waves resulting from dam breaks have been responsible for numerous losses of life. Related situations include flash floods, debris flow surges, glacier lake outburst floods, surging waves in the swash zone, rising tides on dry estuaries and tsunami runup on dry land. For example, Bornschein and Pohl (2003) documented a dam break which induced major damage when the waters surged through the streets of Glashütte township, Germany. The surge front is a shock characterised by a sudden discontinuity and extremely rapid variations of flow depth and velocity. Despite few early studies (Dressler 1954, Escande et al. 1961), current knowledge of dam break wave surging down rough surfaces is still rudimentary and the aerated nature of the advancing surge front remains un-quantified, although clearly evidenced by photographs, movies and witness reports (Fig. 1).

During the present study, flash flood surges were investigated in a large stepped chute. The results provide new information on the wave front propagation. Unsteady two-phase flow measurements were conducted in the surging waters to gain new insights into the air-water flow characteristics.

2. Experimental setup

2.1 Experimental channel

New experiments were performed in the 25 m long 0.5 m wide flume with a slope $S_o \approx 0.065$ ($\theta = 3.4º$) previously used by Chanson (2003) (Table 1). A precise flow rate was delivered by a pump controlled with an adjustable frequency AC motor drive Taian T-Verter K1/N1 (Pulse Width Modulated design), enabling an accurate discharge adjustment in a closed-circuit system. The flow was fed through a smooth convergent nozzle (1.7 m long), and the nozzle exit was 30 mm high and 0.5 m wide. The stepped invert configuration consisted of a 2.4 m long horizontal invert followed by 18 identical steps (h = 0.0715 m, l = 1.2 m).

2.2 Instrumentation

The flow rates in steady flow conditions were measured with a Dall™ tube flowmeter, calibrated on site with a sharp-crested weir. The accuracy on the discharge measurement was about 2%. The surging flow was studied with digital still- and video-cameras using high-shutter speed (1/1,000 to 1/10,000 s) (e.g. Fig. 1).

Fig. 1 - Advancing flood wave down a stepped cascade (h = 0.0715 m, l = 1.2 m)
(A) Q(t=0+) = 0.055 m^3/s, step 16, looking upstream with single-tip conductivity probe array in foreground

(B) Air-water flow structure just behind the flood wave leading edge (Q(t=0+) = 0.065 m^3/s, step 16, looking upstream)

Air-water flow properties were measured with two systems. Air concentrations and bubble count rates were recorded with an array of single-tip conductivity probes (needle probe design). Each probe consisted of a sharpened rod (platinum wire $\varnothing$ = 0.35 mm) which was insulated except for its tip and set into a metal supporting tube (stainless steel surgical needle $\varnothing$ = 1.42 mm) acting as the second electrode. The second apparatus was a double-tip conductivity probe. The inner electrode was a Platinum wire (99.9% purity, $\varnothing$ = 0.15 mm) and the outer electrode was a stainless steel surgical needle ($\varnothing_{int}$ = 0.5 mm, $\varnothing_{ext}$ = 0.8 mm). Each tip was identical and the distance between sensor was Δx_{tip} = 8.9 mm. The probe was

designed with a small frontal area of the first tip (i.e. 0.5 mm^2) and with a displaced second tip (offset: 1.4 mm) to avoid wake disturbance from the leading tip. With both probe systems, the sensors were aligned along the flow direction and excited by an air bubble detector developed at the University of Queensland (UQ82.518) with a response time of less than 10 μs and calibrated with a square wave generator. The probe output signals were scanned at 10 kHz per channel for six seconds.

Data acquisition was triggered manually immediately prior to the flow arrival to have a minimum of 5 seconds of record. Visual observations showed that the wave front was roughly two-dimensional. Measurements were conducted on several steps at several distances x from the step vertical face on the chute centreline. At each location x, a single-tip conductivity probe (i.e. reference probe) was set on the invert, acting as a time reference, while the other probes were set at different elevations (Fig. 2). Each experiment was repeated until sufficient data were obtained for each vertical profile. The displacement of the probes in the direction normal to the invert was controlled by a fine adjustment travelling mechanism. The error in the probe position was less than 0.2 mm and 2 mm in the vertical and horizontal directions respectively.

Table 1 - Summary of unsteady dam break wave flows on initially-dry rough channels

Experiment	θ (deg.)	h m	Q(t=0+) (m^3/s)	Steady flow regime	Remarks
(1)	(2)	(3)	(4)	(5)	(6)
Dressler (1954)	0	0.0056	0.0027 0.0076 0.0215	Skimming	65-m long horizontal channel with strip roughness (h = 0.0056 m, l = 0.0224 m). W = 0.225 m..
Brushes Clough dam	18.4	0.19	0.5	Skimming	Inclined downward steps, trapezoidal channel (2 m bottom width). 1994 test re-analysed by Chanson (2001).
Glashütte dam break	--	--	100 to 200 (at dam)	--	Failure of 9 m high embankment dam on Tues. 12 Aug. 2002 (Bornschein and Pohl 2003).
Chanson (2003) Series 1	3.4	0.143	0.019 to 0.075	Nappe	25 m long sloping channel. 10 horizontal steps (l = 2.4 m). W = 0.5 m. Nozzle depth : d_n = 0.030 m.
Series 2	3.4	0.0715	0.040 to 0.075	Trans./Skim.	18 horizontal steps (l = 1.2 m). W = 0.5 m. Nozzle depth : d_n = 0.030 m.
Present study	3.4	0.0715	0.050 0.060 0.065 0.070	Skimming	18 horizontal steps (l = 1.2 m). W = 0.5 m. Nozzle depth : d_n = 0.030 m.

Notes : Q(t=0+) : initial flow rate; d_n : approach flow depth; h : vertical step height (or roughness height); l : horizontal step length (spacing between roughness); W : channel width.

2.3 Data processing

Steps were painted with red and white stripes spaced 50 mm apart (Fig. 1). Video-taped movies were analysed frame-by-frame. The error on the time was less than 1/250 s and the error on the longitudinal position of the wave front was +/- 1 cm.

The conductivity probe signal outputs were processed using a single threshold technique. The threshold was set at about 50% of air-water voltage range. Unsteady void fractions C and bubble count rates F were calculated during a short time interval τ such as $\tau = \Delta X/V_s$ where

V_s is the surge front celerity measured with the video-cameras and ΔX is the control volume streamwise length. Preliminary tests indicated that the control volume length had to satisfy $\Delta X \geq 70$ mm to contain a minimum of 5 to 20 bubbles (Chanson 2003). The selection was consistent with the processing technique of Stutz and Reboud (2000) in periodic cavitating flow. The bubble count rate was calculated as: $F = N_{ab}/\tau$ where N_{ab} is the number of bubbles detected during the time interval τ. Bubble and water chord times were measured where the bubble chord time t_{ch} is defined as the time spent by the bubble on the probe tip.

Velocity data were calculated from individual droplet/bubbles events impacting successively the two probe sensors. The velocity was deduced from the time lag for air-to-water interface detections between leading and trailing tips respectively. For each meaningful event, the interfacial velocity was calculated as: $V = \Delta x_{tip}/\delta t$ where Δx_{tip} is the distance between probe sensors and δt is the interface travelling time between probe sensors.

The measurement of air-water interface area is a function of the void fraction, velocity, bubble size and bubble count. For any bubble shape, bubble size distribution and chord length distribution, the specific air-water interface area may be estimated as: $a = 4*F/V$.

Fig. 2 - Definition sketch
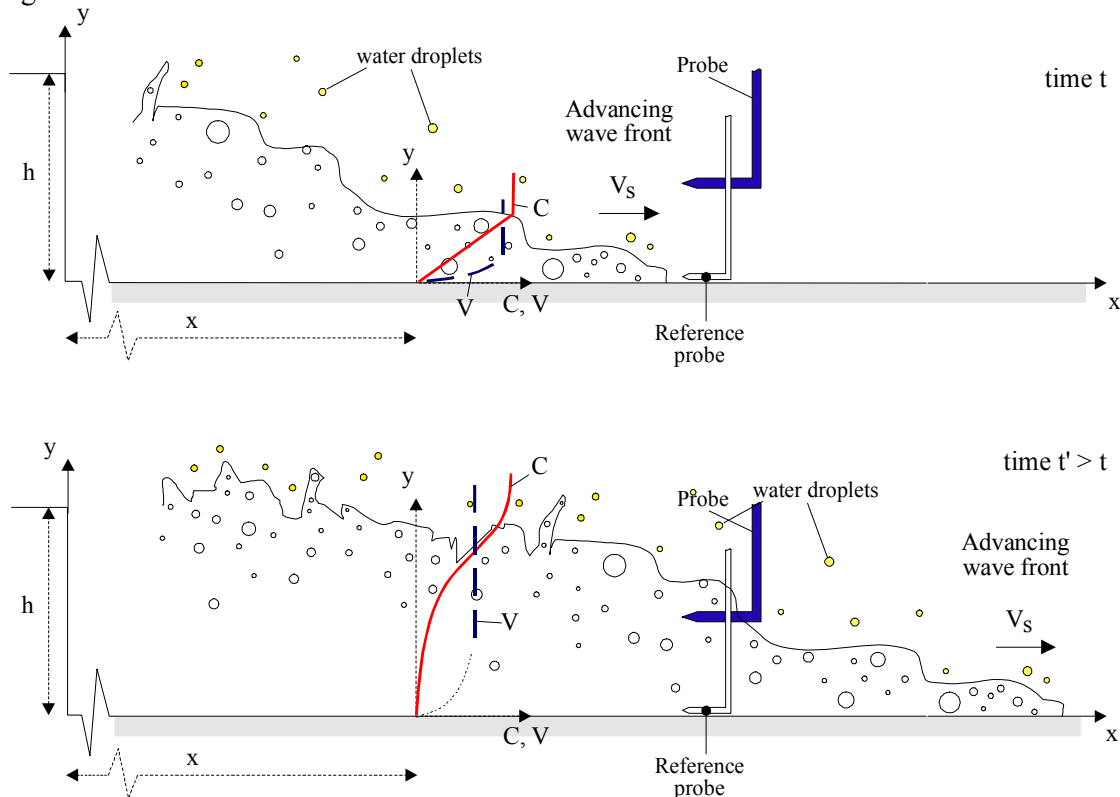
2.4 Boundary flow conditions

Prior to the start of each experiment, the recirculation pipe system and convergent intake were emptied. The channel was initially dry. The pump was rapidly started. The electronic controller had a 5 seconds ramp. The pump reached its nominal power (i.e. flow rate) at least 10 seconds prior to the water entering the channel. The discharge $Q(t=0+)$ was maintained constant until at least 10 seconds after the wave front reached the downstream end of the flume.

Previously, steady flow experiments were conducted in the same channel with smooth and stepped invert configurations (Chanson and Toombes 2002a). These steady air-water flow results provided the limiting conditions of the present study with unsteady flows.

3. Wave front propagation

For all experiments, visual observations showed that the wave front propagated as a succession of free-falling nappe, nappe impact and horizontal runoff (Fig. 1). For comparison, the flow regime observations in steady flows are summarised in Table 1 (column 5). The wave front exhibited a nappe flow behaviour for all flow conditions in all studies down stepped inclined chutes, although steady flow conditions could correspond to transition or skimming flow regimes as defined by Chanson (2001). The wave front was highly aerated, in particular for the larger flow rates (Fig. 1). Figure 1 shows the chaotic nature of wave front, with strong spray, splashing and wavelets. Water packets were commonly projected to heights greater than 3 to 5 step heights, while some droplets reached heights of more than 10 step heights. Visually laboratory experiments in the large-size flume had a similar appearance to prototype surging flows observed during the Brushes Clough dam spillway tests and during the Glashütte dam break wave surging in the township.

The propagation of the wave front was recorded for a range of unsteady flow conditions (Table 1). Wave front celerity data showed some flow acceleration in the first 4 to 6 steps. Further downstream, a gradual decay in celerity was observed. The data were compared successfully with Hunt's (1982) theory for dam break wave down sloping chutes. A fair agreement was achieved assuming an equivalent Darcy-Weisbach friction factor $f = 0.05$, irrespective of flow rate and chute configuration (Chanson 2003, Present study). This flow resistance value is close to air-water flow measurement results in steady flow conditions yielding $f \sim 0.047$ (Chanson and Toombes 2002a).

In the following sections, air-water flow properties are detailed in the horizontal runoff flow region in terms of distributions of void fraction, bubble count rate, turbulent velocity and bubble/droplet sizes.

4. Void fraction and bubble count rate distributions

Typical measurements of instantaneous void fractions, bubble count rate and specific interface area in the horizontal runoff are presented in Figure 3 for different times t at one location x, where t is the time from the first water detection by the reference probe. In Figure 3, d_o is a measure of the initial flow rate $Q(t=0+)$:

$$d_o = \frac{9}{4} * \sqrt[3]{\frac{Q(t=0+)^2}{g * W^2}}$$
(1)

g is the gravity acceleration and W is the chute width. At leading edge, the void fraction distributions had a roughly linear shape :

$$C = 0.9 * \frac{y}{Y_{90}} \qquad\qquad t*\sqrt{g/d_o} < 1.2 \quad (2)$$

where y is the distance normal to the invert and Y_{90} is the height where $C = 0.90$. For larger times t, the distributions of air concentration were best described by the diffusion model :

$$C = 1 - \tanh^2\left(K' - \frac{\frac{y}{Y_{90}}}{2 * D_o} + \frac{\left(\frac{y}{Y_{90}} - \frac{1}{3}\right)^3}{3 * D_o}\right) \qquad t*\sqrt{g/d_o} > 1.5 \quad (3)$$

where K' and D_o are functions of the depth-averaged void fraction C_{mean} only (Chanson and Toombes 2002b), and C_{mean} is defined as :

$$C_{mean} = \frac{1}{Y_{90}} * \int_0^{Y_{90}} C * dy$$
(4)

Fig. 3 - Distributions of instantaneous void fractions, bubble count rate and air-water specific interface area (Q(t=0+) = 0.075 m^3/s, d$_o$ = 0.297 m, , step 16, x = 0.8 m, ΔX = 385 mm)

	0-385 mm	350-735 mm	700-1085 mm	Steady flow
t (s) =	0.079	0.223	0.367	$+\infty$
C$_{mean}$ =	0.46	0.35	0.30	0.24

(A) Dimensionless distributions of void fraction C and air bubble diffusivity D' - Comparison with Equations (2) and (3)
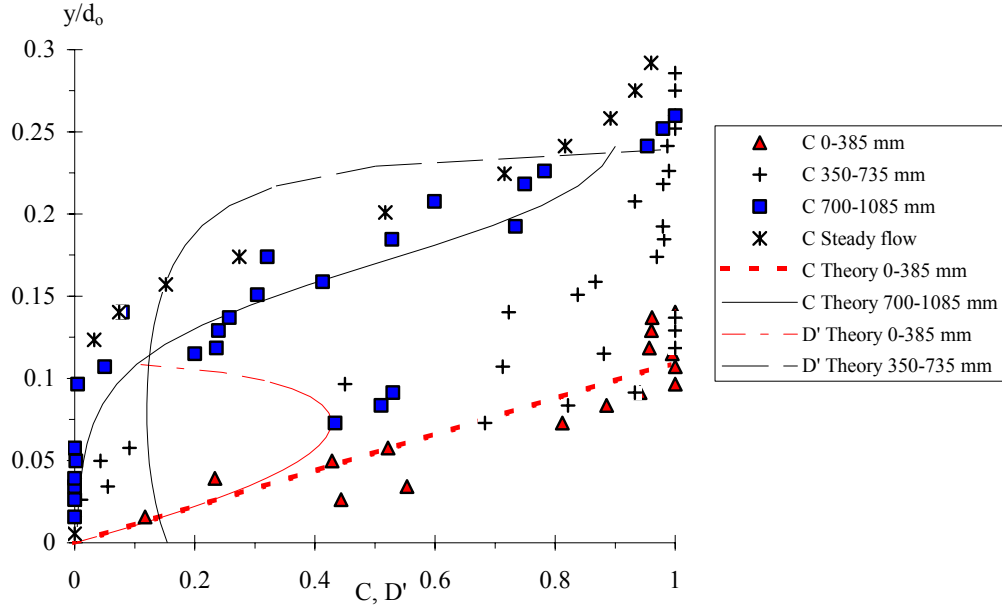
(B) Distributions of bubble count rate F and specific interface area a
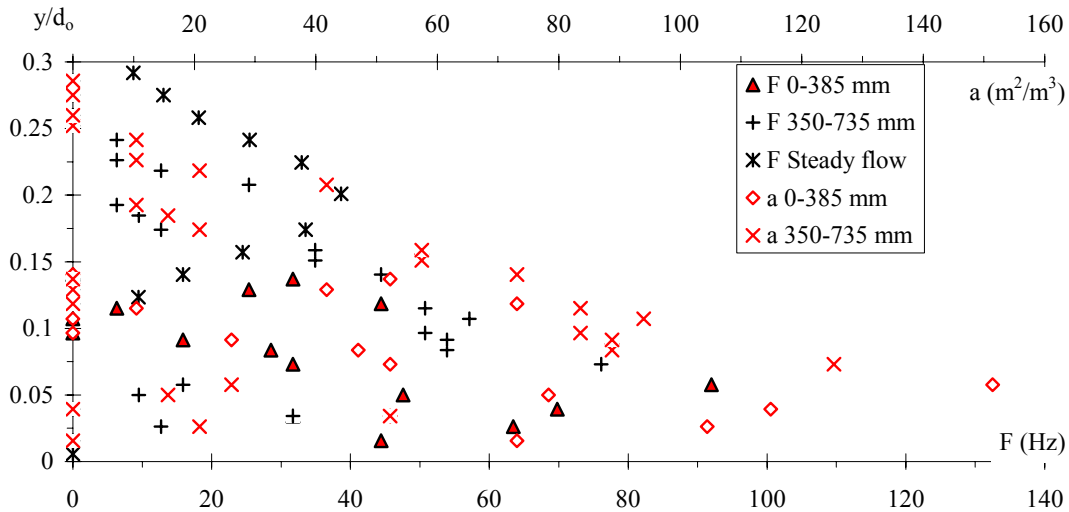
Equations (2) and (3) are plotted for unsteady flow conditions in Figure 3A. They are analytical solutions of the advective diffusion of air bubbles assuming respectively the following distributions of dimensionless turbulent diffusivity of air bubbles:

$$D' = \frac{C * \sqrt{1 - C}}{0.9} \qquad\qquad t*\sqrt{g/d_0} < 1.2 \quad (5)$$

$$D' = \frac{D_O}{1 - 2 * \left(\frac{y}{Y_{90}} - \frac{1}{3}\right)^2} \qquad t^*\sqrt{g/d_O} > 1.5 \quad (6)$$

where $D' = D_t/((u_r)_{Hyd}*\cos\theta*Y_{90})$, D_t is the turbulent diffusivity, $(u_r)_{Hyd}$ is the bubble rise velocity in hydrostatic pressure gradient. Equations (5) and (6) are plotted in Figure 3A in thin dashed lines. The shape of Equation (5) is similar to the sediment diffusivity distribution developed by Rouse (1937) which yields to the Rouse distribution of suspended matter (e.g. Nielsen 1992, Chanson 1999).

Figure 3B presents measured bubble count rate and specific interface area distributions. The scale of the horizontal axes is in dimensional units to emphasise the order of magnitude. Overall the data showed consistently large bubble count rates and interfacial areas at the surge leading edge, while the maximum bubble count rate and interface area decreased with increasing time t towards steady flow values.

Discussion

The data highlighted a significant change in void fraction distribution shape for $t^*\sqrt{g/d_O}$ ~ 1.2 to 1.5. Possible explanations might include a non-hydrostatic pressure field in the leading front of the wave, some change in air-water flow structure between the leading edge and the main flow associated with a change in rheological fluid properties, a gas-liquid flow regime change with some plug/slug flow at the leading edge and a homogenous bubbly flow region behind, and a change in boundary friction between the leading edge and the main flow behind. All these mechanisms would be consistent with high-shutter speed movies of leading edge highlighting very dynamic spray and splashing processes (Fig. 1).

The data demonstrated consistently strong aeration of the surge leading edge, especially within the first 0.3 to 0.7 m behind the wave front (Fig. 2 and 3). For example, the depth-averaged void fraction C_{mean} was 0.77, 0.46, 0.35 and 0.24 at t = 0.014, 0.079, 0.223 and 0.94 s respectively for the flow conditions shown in Figure 3. The result has direct implications in terms of sediment processes at the leading edge of flash floods and swash zone runup on beaches. The large amount of 'white waters' reduces buoyancy and increases the relative density of sediment particles. For example, the relative density of quartz particles increases from 2.65 to 5.3 when the mean void fraction increases from 0 to 50%. The present findings imply lesser sediment transport rate at the leading edge, while heavy sediment particles are more likely to be subjected to bed-load motion rather than suspension.

5. Velocity distributions

Figure 4 presents typical interfacial velocity distributions in the horizontal runoff region. In Figure 4A, each data point represents the velocity of the first air-to-water interface at each location y measured for t < 0.12 s. Figure 4B presents the mean velocity for an entire recording (i.e. for less than 6 s) at each location y. Each data point is the median velocity (or the average velocity if less than ten successful detections occur). In addition the number of successful interface detections is shown for each location. Figure 4C shows the ratio of interfacial velocity standard deviation to mean velocity. For large interface counts, the ratio is the turbulence intensity Tu.

At the wave leading edge, the instantaneous velocity data were successfully compared with an analytical solution of the Navier-Stokes equations (first Stokes problem) for startup flow (Fig. 4A):

$$\frac{V}{U} = \text{erf}\left(\frac{y}{2 * \sqrt{\nu_T * t}}\right) \qquad (7)$$

where U is a free-stream velocity, t is the time, and ν_T is the momentum exchange coefficient (or "eddy viscosity") (App. I). The function erf is the Gaussian error function :
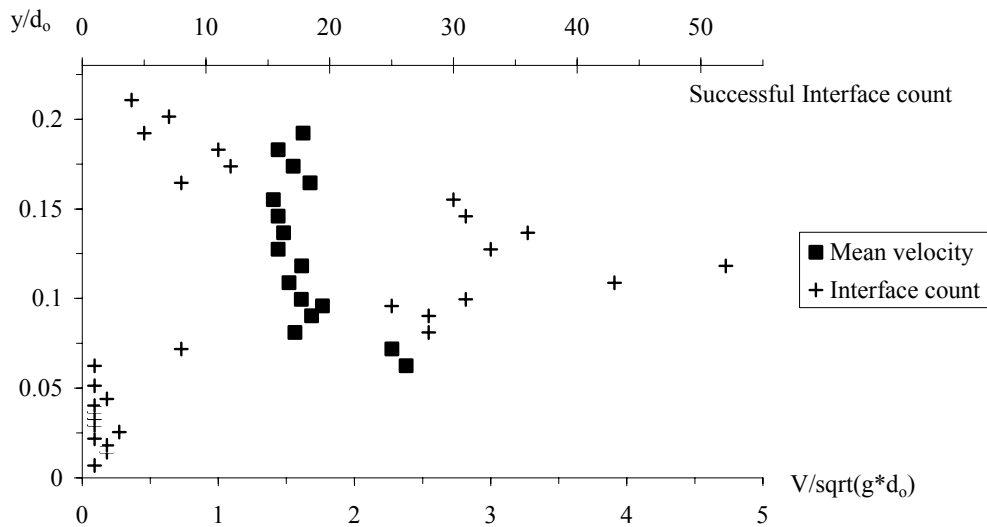
$$\text{erf}(u) \;=\; \frac{2}{\sqrt{\pi}} \;*\; \int_{0}^{u} \exp(-v^2) * dv \tag{8}$$

Fig. 4 - Dimensionless turbulent velocity distributions at the surge leading edge (Q(t=0+) = 0.065 m^3/s, d_o = 0.27 m, step 16, x = 1.0 m)
(A) Interfacial velocity of the first air-to-water interface (t < 0.12 s) - Comparison with Equation (7)
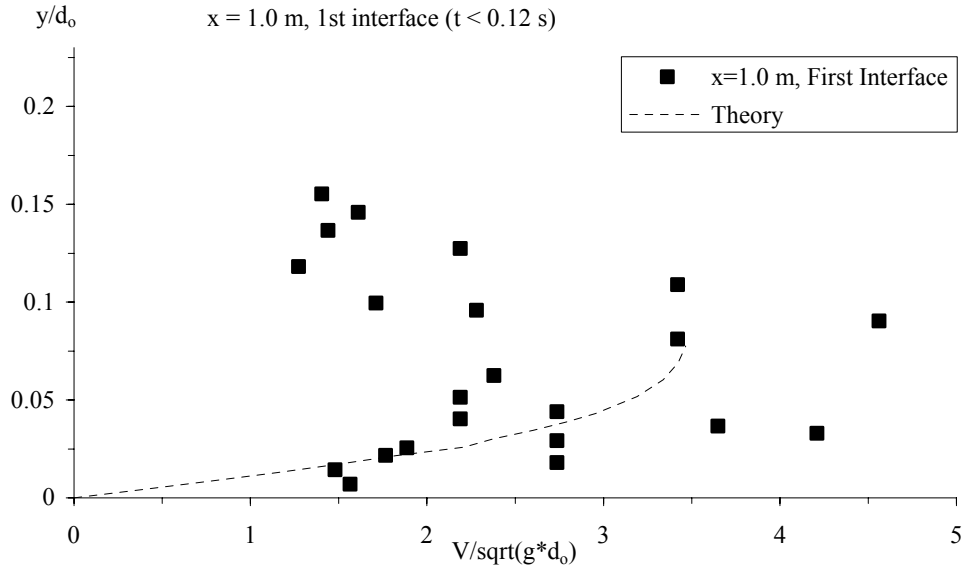
(B) Median interfacial velocity (over about 5 sec.) and number of successful interface detections

(C) Average turbulence intensity (over about 5 sec.) and number of successful interface detections
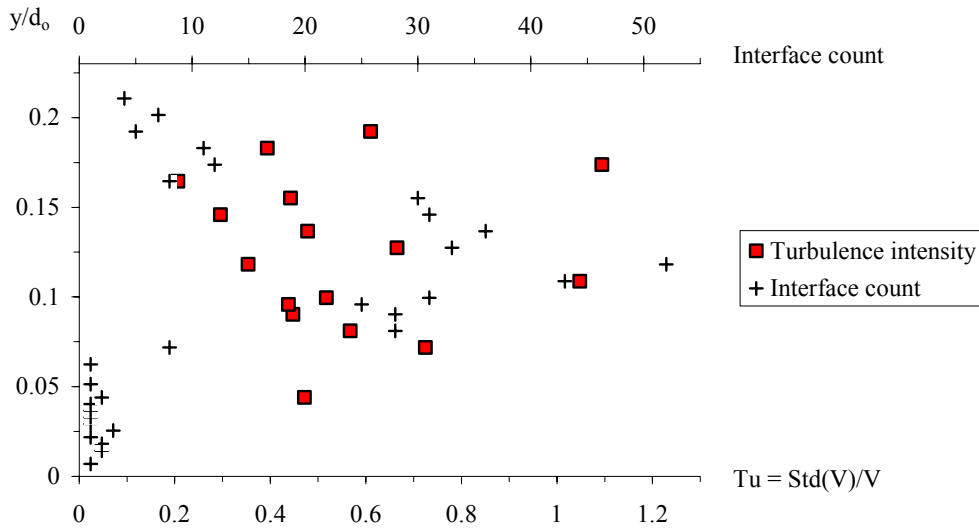

Figures 4B shows that the dimensionless distributions of mean velocity (over about 5 sec.) were quasi-uniform. But the magnitude of the average velocity was consistently smaller than the velocity of the first interface, possibly because of water projections ahead of the surging waters. Figure 4C highlights high levels of turbulence in the surging flow. In Figure 4C, the turbulence levels range from 0.2 to 1.1 with a mean value of about 50%. The values were consistent with turbulence levels measured in steady air-water chute flows (Chanson and Toombes 2002b, Sanchez-Juny et al. 2004). Note, however, that the data were meaningful only for more than 10 successful interface detections (Fig. 4B & 4C).

Discussion
In the horizontal runoff flow and next to the invert, the data highlighted a boundary layer region in the wave leading edge. The finding is consistent with earlier laboratory experiments by Mano (1984) who studied unsteady wave runup using bubble tracer and high speed video, Fujima and Shuto (1990) who performed steady LDA (1 component) measurements on a conveyor belt and Davies (1988) in steady debris flows on a conveyor belt. But Wang (2002), using video observations, recorded a quasi-linear velocity profile at the head of two-phase debris flow, while Jensen et al. (2003) who used PIV technique observed a quasi-uniform velocity profile in wave runup on steep beach (also Wood et al. 2003).
In Equation (7), the values of U and ν_T were determined from best data fit, and they are summarised in Table 2. Despite some scatter and crude approximations leading to Equation (7) (App. I), the results imply a turbulent boundary layer. In wave runup and small to medium debris flows, the boundary layer is believed to be laminar (Mano 1994, Hunt 1994), while the boundary layer is turbulent in prototype dam break wave flows and large debris flows (Witham 1955, Hunt 1984,1988). Based upon present void fraction and velocity measurements, the air bubble diffusivity D_t and eddy viscosity ν_T which satisfy Equations (2) and (7) respectively yielded a ratio D_t/ν_T of about unity in the surge front. The ratio compares the effects of the difference in diffusion of a discrete particle and small coherent fluid structure, as well as the effect of entrained air on the turbulence field (Chanson 1997). The result $D_t/\nu_T \sim 1$ seems to suggest strong interactions between the air bubble diffusion and momentum exchange processes.

Table 2 - Unsteady boundary layer flow characteristics : $Q(t=0+) = 0.065$ m^3/s, Step 16, horizontal runoff flow region

Parameter (1)	x = 0.6 m (2)	x = 0.8 m (3)	x = 1.0 m (4)	Remarks (5)
t (s) =	0.0183	0.0183	0.0281	Experimental values.
B.L. thickness (mm) =	10-12	15-17	20	Rough experimental estimate.
U (m/s) =	4.2	6.0	5.7	Best data fit.
ν_T (m^2/s) =	0.7 E-3	1.25 E-3	1.2 E-3	Best data fit.

6. Air-water flow structures

Air and water chord size measurements highlighted a broad range of bubble and droplet sizes from less than 0.5 mm to more than 30 mm in surging waters. The median air chord sizes were typically between 1 and 10 mm, and the distributions were skewed with a preponderance of smaller bubbles/droplets compared to the mean.

For one flow rate ($Q(t=0+) = 0.075$ m^3/s), a detailed analysis of time variations in air-water flow structure was conducted at several cross-sections in the horizontal runoff flow (i.e. x $\geq$ 0.4 m). A typical example is shown in Figure 5 in terms of median air/water chord sizes calculated for relatively small control volumes ($\tau = 0.158$ s, $\Delta X = 0.385$ m). In Figure 5, the median chord sizes (in mm) are plotted as a function of the relative depth y/Y_{90}. Water chord data are in white symbols while air chord data are in dark symbols. At the wave leading edge, air and water chord sizes were comparable with median sizes of about 3-6 mm (Fig. 5A). This might suggest that individual bubble entrainment was associated with the ejection of water droplet of similar size. For larger times (i.e. $t^*\sqrt{g/d_O} > 0.5$), the order of magnitude of median air chord sizes remained basically constant and independent of time, while median water chord sizes tended to increase with time, especially for $y/Y_{90} < 0.7$ (Fig. 5B). Such a behaviour might be related to fundamental differences between air bubbles and water droplets.

Water droplets have a momentum response time about 46,000 times larger than that of an air bubble of identical diameter (e.g. Crowe et al. 1998). As the bubble response time is significantly smaller than the characteristic time of the flow, bubble trapping in large vortices is a dominant process : bubbles may remain trapped for very long times, the bubbly flow structure has some memory of its past, and it is affected by its previous structure. In the spray region, drop formation results from surface distortion, tip-streaming of ligaments and interactions between eddies and free-surface (e.g. Hoyt and Taylor 1977, Rein 1998). Once ejected, the droplet response time is nearly two orders of magnitude larger the air flow response time. Most droplets have a short life and the spray region has little memory of its past. The spray structure may then change very rapidly in response to changes in flow conditions, while the bubbly flow region is deeply affected by its earlier structure.
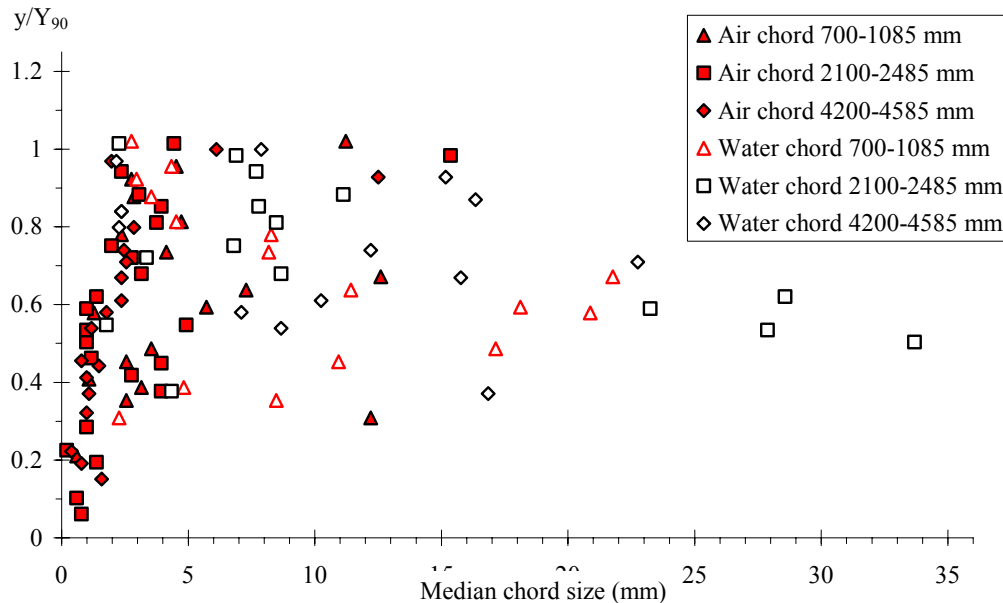
Fig. 5 - Vertical distributions of median chord sizes in small streamwise control volumes at several times t - $Q(t=0+) = 0.075$ m^3/s, Step 16, $x = 0.8$ m, $\Delta X = 385$ mm

	0-385 mm	350-735 mm	700-1085 mm	2100-2485 mm	4200-4585 mm
t (s) =	0.079	0.223	0.367	0.943	1.807

(A)
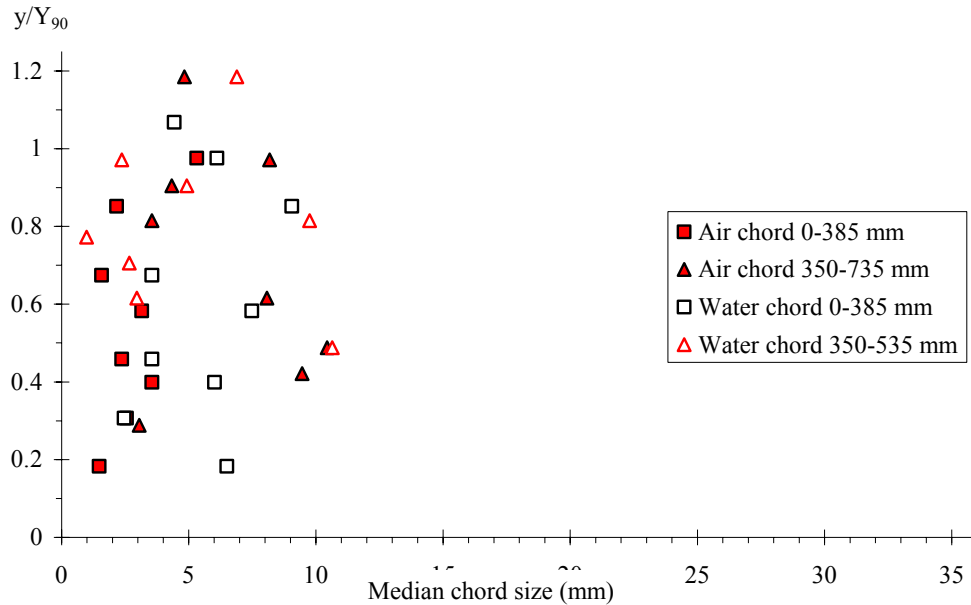
(B)

7. Conclusions

New flood wave experiments were conducted systematically down a 25 m long waterway with a stepped invert. Unsteady air-water flow measurements were performed in the surging waters using an array of resistivity probes. A new processing technique was developed to analyse the probe outputs yielding quasi-instantaneous air-water flow properties.

Application to dam break wave flows demonstrated the soundness of the metrology technique. Results showed quantitatively the strong aeration of the leading edge, although the flow properties tended rapidly towards steady flow characteristics. Void fraction distributions

showed a marked change in shape for $(t - t_S)*\sqrt{g/d_O} \sim 1.3$. Several explanations were proposed. The data showed further the presence of a turbulent boundary layer next to the invert. Measurements of air and water chord sizes highlighted a wide range of bubble and droplet sizes. Time-variations of air-water flow structure were observed. Overall the results emphasised the complicated nature of the dam break wave flow and its leading edge. In practice, the strong aeration of the surge front has some impact on sediment motion near the leading edge, because the sediment relative density is inversely proportional to the air and water fluid density.

It must be emphasised that present results were focused on the horizontal runoff flow. In the free-jet and at nappe impact, preliminary analysis suggested that the unsteady flow structure was significantly more complicated.

8. Acknowledgements

9. Appendix I. Analytical solution of the Navier-Stokes equations in dam break wave front

In the horizontal runoff zone, the boundary layer development at the leading edge of the surge is somehow similar to a startup flow. The analytical solution of the Navier-Stokes equations for unsteady plane laminar flows is called the first Stokes problem or Rayleigh problem after Stokes (1856) and Rayleigh (1911) respectively (Schlichting and Gersten 2000, pp. 126-128).

In the start-up flow, the velocity is independent of the x co-ordinate in the flow direction and the continuity equation yields $V_y = 0$. For a laminar flow, the Navier-Stokes equations become :

$$\rho * \frac{\partial V_x}{\partial t} = -\rho * g * \frac{\partial z}{\partial x} - \frac{\partial P}{\partial x} + \mu * \frac{\partial^2 V_x}{\partial y^2} \tag{I-1a}$$

$$0 = -\rho * g * \frac{\partial z}{\partial y} - \frac{\partial P}{\partial y} \tag{I-1b}$$

where ρ and μ are the fluid density and dynamic viscosity respectively, z is the vertical elevation and P is the pressure. For a horizontal flow, the gravity force component in the flow direction is zero. The Navier Stokes equations yield :

$$\frac{\partial V_x}{\partial t} = \nu * \frac{\partial^2 V_x}{\partial y^2} \tag{I-2}$$

where ν is the kinematic viscosity. Equation (I-2) is similar to a diffusion equation and a heat conduction equation. Mathematical solutions of diffusion and heat equations were addressed in two classical references (Carslaw and Jaeger 1959, Crank 1956).

For an advancing surge flow, the boundary conditions are : $V_x = U$ for $y \geq 0$ and $t \leq 0$, and $V_x(y=0) = 0$ and $V_x(y\rightarrow+\infty) = U$ for $t > 0$. The analytical solution of Equation (I-2) is :

$$\frac{V_x}{U} = \mathrm{erf}\left(\frac{y}{2 * \sqrt{\nu * t}}\right) \tag{I-3}$$

where y is the distance normal to the invert and the function erf is the Gaussian error function defined as :

$$\mathrm{erf}(u) = \frac{2}{\sqrt{\pi}} * \int_0^u \exp(-\tau^2) * d\tau \tag{I-4}$$

The reasoning may be extended to unsteady turbulent boundary layer flow with constant momentum exchange coefficient (or "eddy viscosity") ν_T. The analytical solution of the

Navier-Stokes equations becomes :

$$\frac{V_x}{U} = \text{erf}\left(\frac{y}{2 * \sqrt{\nu_T * t}}\right) \tag{I-5}$$

10. References

BORNSCHEIN, A., and POHL, R. (2003). "Dam Break during the Flood in Saxon/Germay in August 2002." *Proc. 30th IAHR Biennial Congress*, Thessaloniki, Greece, J. GANOULIS and P. PRINOS Ed., Vol. C2, pp. 229-236.

CARSLAW, H.S., and JAEGER, J.C. (1959). "Conduction of Heat in Solids." *Oxford University Press*, London, UK, 2nd ed., 510 pages.

CHANSON, H. (1997). "Air Bubble Entrainment in Free-Surface Turbulent Shear Flows." *Academic Press*, London, UK, 401 pages.

CHANSON, H. (1999). "The Hydraulics of Open Channel Flows : An Introduction." *Butterworth-Heinemann*, Oxford, UK, 512 pages.

CHANSON, H. (2001). "The Hydraulics of Stepped Chutes and Spillways." *Balkema*, Lisse, The Netherlands, 418 pages.

CHANSON, H. (2003). "Sudden Flood Release down a Stepped Cascade. Unsteady Air-Water Flow Measurements. Applications to Wave Run-up, Flash Flood and Dam Break Wave." *Report CH51/03*, Dept of Civil Eng., Univ. of Queensland, Brisbane, Australia, 142 pages.

CHANSON, H., and TOOMBES, L. (2002a). "Energy Dissipation and Air Entrainment in a Stepped Storm Waterway: an Experimental Study." *Jl of Irrigation and Drainage Engrg.*, ASCE, Vol. 128, No. 5, pp. 305-315.

CHANSON, H., and TOOMBES, L. (2002b). "Air-Water Flows down Stepped Chutes : Turbulence and Flow Structure Observations." *Intl Jl of Multiphase Flow*, Vol. 27, No. 11, pp. 1737-1761.

CRANK, J. (1956). "The Mathematics of Diffusion." *Oxford University Press*, London, UK.

CROWE, C., SOMMERFIELD, M., and TSUJI, Y. (1998). "Multiphase Flows with Droplets and Particles." *CRC Press*, Boca Raton, USA, 471 pages.

DAVIES, T.R.H. (1988). "Debris Flow Surges - A Laboratory Investigation." *Mitteilungen der Versuchsanstalt fur Wasserbau, Hydrologie und Glaziologie*, No. 96, ETH-Zurich, Switzerland, 122 pages.

DRESSLER, R. (1954). "Comparison of Theories and Experiments for the Hydraulic Dam-Break Wave." *Proc. Intl Assoc. of Scientific Hydrology Assemblée Générale*, Rome, Italy, Vol. 3, No. 38, pp. 319-328.

ESCANDE, L., NOUGARO, J., CASTEX, L., and BARTHET, H. (1961). "Influence de Quelques Paramètres sur une Onde de Crue Subite à l'Aval d'un Barrage." ('The Influence of certain Parameters on a Sudden Flood Wave Downstream from a Dam.') *Jl La Houille Blanche*, No. 5, pp. 565-575 (in French).

FUJIMA, K., and SHUTO, N. (1990). "Formulation of Frictions Laws for Long Waves on a Smooth Dry Bed." *Coastal Engineering in Japan*, Vol. 33, No. 1, pp. 25-47.

HOYT, J.W., and TAYLOR, J.J. (1977). "Turbulence Structure in a Water Jet Discharging in Air." *Physics of Fluids*, Vol. 20, No. 10, Pt. II, Oct., pp. S253-S257.

HUNT, B. (1982). "Asymptotic Solution for Dam-Break Problems." *Jl of Hyd. Div.*, Proceedings, ASCE, Vol. 108, No. HY1, pp. 115-126.

HUNT, B. (1984). "Perturbation Solution for Dam Break Floods." *Jl of Hyd. Engrg.*, ASCE, Vol. 110, No. 8, pp. 1058-1071.

HUNT, B. (1988). "An Asymptotic Solution for Dam Break Floods in Sloping Channels." in "Civil Engineering Practice", *Technomic Publ.*, Editors P.N. CHEREMISINOFF, N.P. CHEREMISINOFF and S.L. CHENG, Lancaster Pen., USA, Lancaster, USA, Vol. 2, Section 1, Chapter 1, pp. 3-11.

HUNT, B. (1994). "Newtonian Fluid Mechanics Treatment of Debris Flows and Avalanches." *Jl of Hyd. Engrg.*, ASCE, Vol. 120, No. 12, pp. 1350-1363.

JENSEN, A., PEDERSEN, G.K., and WOOD, D.J. (2003). "An Experimental Study of Wave Run-up on a Steep Beach." *Jl of Fluid Mech.*, Vol. 486, pp. 166-188.

MANO, A. (1994). "Boundary Layer Developed near Surging Front." *Coastal Engineering in Japan*, Vol. 37, No. 1, pp. 23-39.

NIELSEN, P. (1992). "Coastal Bottom Boundary Layers and Sediment Transport." *Advanced Series on Ocean Eng.*, Vol. 4, World Scientific Publ., Singapore.

RAYLEIGH, Lord (1911). "On the Motion of Solid Bodies through Viscous Liquids." *Phil. Mag.*, Vol. 21, pp. 697-711.

REIN, M. (1998). "Turbulent Open-Channel Flows : Drop-Generation and Self-Aeration." *Jl of Hyd. Engrg.*, ASCE, Vol. 124, No.1, pp. 98-102. Discussion : Vol. 125, No. 6, pp. 668-670.

ROUSE, H. (1937). "Modern Conceptions of the Mechanics of Turbulence." *Transactions*, ASCE, Vol. 102, pp. 463-543.

AMADOR, A., SÁNCHEZ-JUNY, M., DOLZ, J., SANCHEZ-TEMBLEQUE, F., and PUERTAS, J. (2004). "Velocity and Pressure Field in Skimming Flow in Stepped Spillways." *Proc. Intl Conf. on Hydraulics of Dams and River Structures*, Tehran, Iran, Balkema Publ. The Netherlands, 8 pages.

SCHLICHTING, H., and GERSTEN, K. (2000). "Boundary Layer Theory." *Springer Verlag*, Berlin, Germany, 8th edition., 707 pages.

STOKES, G.G. (1856). "On the effect of Internal Friction of Fluids on the Motion of Pendulums." *Trans. Camb. Phil. Soc.*, Vol. 9, Part II, pp. 8-106.

STUTZ, B., and REBOUD, J.L. (2000). "Measurements within Unsteady Cavitation." *Experiments in Fluids*, Vol. 29, pp. 545-552.

WANG, Z.Y. (2002). "Initiation and Mechanism of Two Phase Debris Flow." *Proc. Conf. on Flood Defence'2002*, Ed. WU et al., Science Press, New York, pp. 1637-1648.

WITHAM, G.B. (1955). "The Effects of Hydraulic Resistance in the Dam-Break Problem." *Proc. Roy. Soc. of London*, Ser. A, Vol. 227, pp. 399-407.

WOOD, D.J., PEDERSEN, G.K., and JENSEN, A. (2003). "Modelling of Run-up of Steep Non-Breaking Waves." *Ocean Eng.*, Vol. 30, pp. 625-644.